Thermo X

Science Exploration

Open Access Research Article

Vertically channeled GO/LiCl photothermal hydrogel via directional freezing for high-efficiency solar atmospheric water harvesting

Jiaxue Yu[1,2], Debing Wang[1,2], Yifan Li[1,2,*], Huaqing Xie[1,2], Wei Yu[1,2], Lingling Wang[1,2,*]

[1]School of Energy and Materials, Shanghai Polytechnic University, Shanghai 201209, China.
[2]Shanghai Engineering Research Center of Advanced Thermal Functional Materials, Shanghai Polytechnic University, Shanghai 201209, China.

***Correspondence to:** Yifan Li, School of Energy and Materials, Shanghai Polytechnic University, Shanghai 201209, China; Shanghai Engineering Research Center of Advanced Thermal Functional Materials, Shanghai Polytechnic University, Shanghai 201209, China. E-mail: liyf@sspu.edu.cn

Lingling Wang, School of Energy and Materials, Shanghai Polytechnic University, Shanghai 201209, China; Shanghai Engineering Research Center of Advanced Thermal Functional Materials, Shanghai Polytechnic University, Shanghai 201209, China. E-mail: llwang@sspu.edu.cn

Received: August 04, 2026 **Accepted:** October 15, 2026 **Published:** October 16, 2026

Cite this article: Yu J, Wang D, Li Y, Xie H, Yu W, Wang L. Vertically channeled GO/LiCl photothermal hydrogel via directional freezing for high-efficiency solar atmospheric water harvesting. Thermo-X. 2027;3:202634. https://doi.org/10.70401/tx.2026.0038

Abstract

Freshwater scarcity has become a severe global crisis, and sorption-based atmospheric water harvesting (SAWH) is a promising solution. Traditional lithium chloride-based hygroscopic hydrogels suffer from sluggish adsorption-desorption kinetics caused by disordered pore channels and insufficient internal mass transfer. In this work, a photothermal hygroscopic hydrogel (DFHG-Li) with vertically aligned directional channels is synthesized through directional freezing-assisted polymerization. Directed ice templates create unobstructed mass transfer tunnels, graphene oxide endows excellent solar-to-thermal conversion performance, and evenly anchored LiCl offers abundant water capture sites. Characterizations confirm complete pore integrity and uniform salt distribution. Optimized DFHG-Li reaches swelling equilibrium in merely 3 min and delivers a high water uptake of 3.37 g g^{-1} at 90% RH. Under 1 sun irradiation, its surface temperature rises to 51.2 °C within 15 min, achieving a desorption efficiency of 91.5% in 70 min. After 20 adsorption-desorption cycles, over 89% of its initial water absorption capacity is maintained. This work provides an effective structural regulation strategy to boost mass transfer for high-efficiency solar-driven atmospheric water harvesting.

Keywords: Atmospheric water harvesting, directional freezing, photothermal hydrogel, lithium chloride, graphene oxide, mass transfer

1. Introduction

Global freshwater scarcity poses a major threat to human sustainable development, given that merely 2.5% of Earth's water is accessible freshwater and over two-thirds of this fraction is trapped within glaciers and deep underground aquifers[1]. With continued global population growth, accelerating industrialization, and intensifying climate change, water pollution and the imbalance between water supply and demand are becoming increasingly prominent[2]. It is projected that by 2050, more than 50% of the global population will face freshwater scarcity[3]. In this context, the approximately 12.9 trillion tons of water vapor present in the atmosphere represent a potential renewable freshwater source, and its exploitation and utilization are regarded as a promising approach to alleviating the global water crisis[4,5].

Sorption-based atmospheric water harvesting (SAWH) technology has emerged as a research hotspot owing to its unique advantages, including broad humidity applicability, decentralized deployability, and low energy consumption, without being constrained by geographical and climatic conditions[6]. The core of this technology lies in the capture and conversion of water vapor through the adsorption-desorption cycles of sorbents, whose performance directly determines the freshwater yield and energy efficiency of the water harvesting system[7]. In recent years, various high-performance sorbents have been developed, including metal-organic frameworks (MOFs), covalent organic frameworks (COFs), and hygroscopic salt-based composite materials[8]. Among these, hygroscopic salt-hydrogel composites (HSHCs) offer a compelling combination of fast adsorption kinetics, high water storage, and structural stability. The hydrogel matrix confines hygroscopic salts (e.g., LiCl) to boost adsorption performance while simultaneously preventing salt leakage[9]. Furthermore, through the molecular design of the hydrogel network, precise regulation of adsorption

© The Author(s) 2026. This is an Open Access article licensed under a Creative Commons Attribution 4.0 International License (https://creativecommons.org/licenses/by/4.0/), which permits unrestricted use, sharing, adaptation, distribution and reproduction in any medium or format, for any purpose, even commercially, as long as you give appropriate credit to the original author(s) and the source, provide a link to the Creative Commons license, and indicate if changes were made.

capacity or desorption energy consumption can be realized[10]. Graeber *et al.* investigated LiCl-doped polyacrylamide non-porous homogeneous hygroscopic hydrogels, which were fabricated via solution crosslinking, and systematically analyzed their water vapor transport behavior[11]. This salt-doped system achieved high water vapor adsorption capacity under moderate-to-high humidity conditions; however, the dense homogeneous network imposed substantial diffusional resistance to water molecules within the interior, resulting in poor adsorption-desorption kinetics and prolonged equilibration time[12]. To improve mass transfer efficiency, the foaming method has been explored to construct porous structures within the hydrogel, wherein randomly distributed macropores are generated using bubble templates to increase the contact area with water vapor, thereby accelerating the moisture capture rate to some extent. For example, Song *et al.* employed mechanical foaming combined with *in situ* polymerization to fabricate a PAM/PVA double-network hygroscopic hydrogel with a layered porous structure, achieving an adsorption capacity of 0.785–3.507 g/g over a broad humidity range of 30%–90%[13]. However, Zhao *et al.* systematically pointed out in their review that porous polymeric materials prepared by the foaming method often suffer from poor pore interconnectivity, tortuous mass transfer pathways, and issues such as pore collapse and localized salt agglomeration during cyclic operation, which compromise their long-term service stability[14]. To overcome these limitations, the cryogelation method employs ice-crystal templating to construct continuous macroporous networks, effectively reducing diffusional resistance[15,16]. However, non-directional freezing results in honeycomb-like pore morphology with lower pore connectivity compared to the lamellar structure obtained by unidirectional freezing[17]. Hence, precise fabrication of directionally ordered pore channels is critical for optimizing cryogel-based hygroscopic hydrogels[18,19].

It is worth noting that the construction of interconnected and ordered pore channels through the regulation of directional ice crystal growth has been demonstrated as an effective strategy to alleviate the mass transfer resistance of water vapor in hygroscopic hydrogels and to overcome the bottleneck of adsorption kinetics[20]. Beyond atmospheric water harvesting, such vertically aligned channel architecture also enables enhanced performance for other gas-treatment applications. For instance, Fang *et al.* reported that multi-scale micro-nano channels fabricated by directional freezing greatly boost mass-transfer efficiency, realizing 83.8% formaldehyde removal within 12 h, which is 60.8% faster than the counterpart without aligned channels[21]. With respect to the regulatory role of directional pore channels on mass transfer behavior, Entezari *et al.* fabricated a binary hydrophilic polymer salt/functionalized multi-walled carbon nanotube (FCNT) composite hydrogel by using sodium alginate as the matrix, modifying it with Li^+ and Ca^{2+} to increase adsorption sites, and incorporating FCNTs to enhance photothermal absorption, achieving an adsorption capacity of 5.6 g/g at 70% relative humidity[22]. Li *et al.* prepared polyvinyl alcohol/sodium alginate composite aerogels via directional freezing, using carbon nanotubes as the photothermal absorber, which achieved a light absorption rate as high as 97% and a water evaporation rate of 2.7 $kg \cdot m^{-2} \cdot h^{-1}$ under one sun illumination[23].

To meet the application demand for solar-driven *in situ* regeneration, photothermal functionalization has become the mainstream modification strategy for directional hygroscopic hydrogels[24,25]. Liu *et al.* confirmed that integrating broadband photothermal mediators such as carbon nanotubes, MXene, and graphene oxide with LiCl lowers desorption activation energy and improves water release efficiency under light irradiation[26]. Following this rationale, Zhu *et al.* demonstrated the feasibility of integrating directional pore channels with photothermal fillers by fabricating cellulose nanofiber/LiCl composite adsorbents via 3D printing combined with freeze-drying, which achieved 1.6-fold higher adsorption rate and 2.4-fold higher release rate than conventional freeze-dried aerogels[27]. However, this approach still faces common bottlenecks in achieving long-term cyclic stability. Li *et al.* developed bacterial cellulose/sodium alginate/graphene oxide/lithium chloride (BC/SA/GO-LiCl) aerogels via directional freezing, which achieved adsorption capacities of 1.4–5.7 $g \cdot g^{-1}$ over a relative humidity range of 30%–90%[28]. Nevertheless, the crosslinked network based on a single-network polymer matrix is prone to skeleton shrinkage and deformation under high LiCl loading and repeated adsorption-desorption cycles[29]. Thus, although current research has made progress in the integration of directional pore channels and photothermal functionality, how to simultaneously ensure cyclic structural stability on the basis of efficient mass transfer and photothermal desorption remains a core challenge that urgently needs to be addressed in this field[30,31].

To address the low mass transfer efficiency of conventional freeze-cast hydrogels and the insufficient synergy of photothermal regeneration and cyclic stability in existing directional materials, this study proposes a directional freezing-assisted polymerization strategy to fabricate a graphene oxide-modified photothermal hygroscopic hydrogel with vertically aligned channels (DFHG-Li). Unlike non-directional freezing, a unidirectional temperature gradient is established via a bottom copper plate to induce vertical ice crystal growth, leaving continuous channels that serve as rapid pathways for water vapor and salt solution transport after thawing. GO is incorporated to enable broadband photothermal conversion for solar-driven desorption at reduced energy cost. The DFHG-Li was synthesized from acrylamide (AM) and N,N'-methylenebisacrylamide (MBAA) via directional freezing *in situ* polymerization, followed by LiCl immersion loading, yielding a composite sorbent with fast adsorption, efficient photothermal desorption, and robust cyclic stability. Systematic characterization of the microstructure, composition, mechanical/thermal properties, and adsorption-desorption kinetics was conducted to unravel the regulatory mechanisms of directional channels and photothermal-hygroscopic synergy on water harvesting performance. This integrated strategy offers a new paradigm for overcoming the dual bottlenecks of poor mass transfer and high regeneration energy in HSHCs, paving the way toward low-cost, practical solar-driven atmospheric water harvesting.

2. Methods

2.1 Materials

AM (≥ 99.0%), MBAA (≥ 95.0%), and LiCl (analytical grade, ≥ 99.0%) were purchased from Shanghai Titan Scientific Co., Ltd. Ammonium persulfate (APS, ≥ 98.0%) was supplied by Sinopharm Chemical Reagent Co., Ltd., and graphene oxide was obtained from Hangzhou Gaoxi Technology Co., Ltd. All reagents were used as received without any further purification.

2.2 Preparation of directionally frozen hydrogels (DFH, DFHG, and DFHG-Li)

For the preparation of DFH, 0.02 g of MBAA and varying amounts of AM (6 wt%, 9 wt%, and 12 wt%) were dissolved in 10 mL of deionized water under stirring at 500 rpm for 30 min at room temperature. Subsequently, 0.04 g of APS was added and stirred for 1 min. The resulting solution was poured into a polytetrafluoroethylene (PTFE) mold equipped with a copper plate at the bottom, and then frozen at -20 °C for 3 h to induce directional growth of ice crystals, followed by polymerization at -5 °C for 12 h. The obtained samples were designated according to the AM content. For the preparation of DFHG, 15 mg of GO powder was added to the precursor solution and stirred at 500 rpm for more than 1 h at room temperature to form a homogeneous suspension, after which the subsequent procedures were identical to those for DFH. The as-prepared products were rinsed with deionized water three times to remove residual reagents. For the preparation of DFHG-Li, the DFHG samples dried to constant weight were immersed in LiCl aqueous solutions of varying concentrations (optimally 10 wt%) for 48 h. After reaching adsorption saturation, the samples were dried in an oven at 60 °C to constant weight. The final products were designated according to the AM content and LiCl concentration.

2.3 Preparation of conventional hygroscopic hydrogel (CHG-Li)

For comparative performance evaluation, a homogeneous solution containing AM, MBAA, GO, and APS was prepared following the same precursor formulation as that of DFHG. Instead of undergoing freezing pretreatment, the solution was directly poured into a PTFE mold and subjected to thermal polymerization in an oven at 80 °C for 2 h to obtain CHG. After rinsing with deionized water, the CHG was immersed in a 10 wt% LiCl solution for 48 h and then dried at 60 °C to constant weight, yielding CHG-Li.

2.4 Characterization and performance testing

The morphology and elemental distribution of samples were observed by scanning electron microscopy coupled with energy dispersive X-ray spectroscopy (SEM-EDS, Apreo 2S, Thermo Fisher Scientific, USA). X-ray diffraction (XRD) patterns were collected on an X-ray diffractometer (XRD 6100, Shimadzu, Japan). Fourier transform infrared (FTIR) spectra were acquired using a Nicolet IS 10 spectrometer (Thermo Fisher Scientific, USA). Thermogravimetric analysis (TG/DTG) was carried out on a STA 449 F3 thermal gravimetric analyzer (NETZSCH, Germany). UV-Vis-NIR absorption spectra were measured by a Lambda 950 spectrophotometer (PerkinElmer, USA). Solar illumination was simulated with an HM-Xe 500W xenon-lamp solar simulator (Zhongjiao Jinyuan, China). Surface temperature was recorded by a Ti401 PRO infrared thermal imager (Fluke, USA). Hygroscopic tests were performed in a SETH-S-020R constant temperature-humidity chamber (Espec, Japan).

For swelling performance testing, cuboid samples with dimensions of 10 × 10 × 5 mm were used for swelling measurement. The DFHG-Li and CHG-Li samples dried to constant weight (initial mass recorded as m_0) were immersed in a 10 wt% LiCl solution at 25 °C, and the sample mass (recorded as m_t) was periodically measured until no further changes were observed after 10 min. The swelling ratio (SR) was calculated according to Equation (1), and the swelling kinetic curves were plotted accordingly[32]:

$$SR = \frac{m_t - m_0}{m_0} \times 100\% \quad (1)$$

where SR is the swelling ratio (%), m_t is the real-time mass of the sample (g), and m_0 is the initial dry mass of the sample (g).

For hygroscopic performance testing, rectangular samples (10 × 10 × 5 mm) were employed for hygroscopic, photothermal desorption and cyclic stability tests. The DFHG-Li and CHG-Li samples dried to constant weight (initial mass recorded as m_0) were placed in a constant temperature and humidity chamber under different relative humidity conditions (30%, 50%, 70%, and 90%) at 25 °C. The sample mass (recorded as m_t) was weighed at 1 h intervals until the mass change rate fell below 0.05%, indicating that hygroscopic equilibrium had been reached. The water uptake (W) was then calculated according to Equation (2)[33]:

$$W = \frac{m_t - m_0}{m_0} \quad (2)$$

where W is the water uptake (g/g), m_t is the real-time mass of the sample (g), and m_0 is the initial dry mass of the sample (g). Additionally, the effects of varying AM content (0.6 g, 0.9 g, and 1.2 g) and LiCl concentration (5 wt%, 10 wt%, 20 wt%, and 30 wt%) on the hygroscopic performance were investigated, and the corresponding hygroscopic kinetic curves were plotted.

For photothermal conversion and desorption performance testing, the light absorption spectra of DFHG-Li and CHG-Li were measured using a UV-Vis-NIR spectrophotometer over the wavelength range of 300-1,400 nm to evaluate the light absorption

efficiency of GO. The moisture-saturated samples were then placed under a xenon lamp solar simulator at different light intensities (0.5, 1.0, and 1.5 sun), and the surface temperature was monitored in real time using an infrared thermal imager to record the temperature-time curves for assessing the photothermal conversion efficiency. One sun illumination corresponds to a solar irradiance of 1 kW m^{-2}. For desorption performance testing, the moisture-saturated samples (initial mass recorded as m_s) were placed on an electronic balance and subjected to desorption experiments under solar illumination of varying intensities. The sample mass (recorded as m_n) was recorded at 1 min intervals, and the desorption rate (D) was calculated according to Equation (3)[33,34]:

$$D = \frac{m_s - m_n}{m_s - m_0} \times 100\% \quad (3)$$

where D is the desorption rate (%), m_s is the mass of the moisture-saturated sample (g), m_n is the real-time mass during the desorption process (g), and m_0 is the initial dry mass of the sample (g).

3. Results and Discussion

3.1 Microstructural morphology analysis

The preparation of DFHG-Li integrates directional freezing technology, *in situ* polymerization, and hygroscopic salt loading, and the corresponding preparation mechanism is illustrated in Figure 1. At -20 °C, the water in the hydrogel precursor solution undergoes directional growth into oriented ice crystals along the vertical direction, driven by the directional thermal conduction of the copper plate at the bottom. Concurrently, APS initiates the *in situ* polymerization of AM monomers with MBAA crosslinker to form the polymer network. The temperature is then raised to -5 °C to allow further reaction. Upon thawing, the ice crystals melt away, leaving behind a hydrogel with a directionally aligned channel structure *in situ*. GO is uniformly dispersed throughout the network to impart photothermal properties. Finally, immersion in a LiCl solution enables the loading of the hygroscopic salt into both the hydrogel network and the directional channels, successfully yielding the DFHG-Li hygroscopic hydrogel.

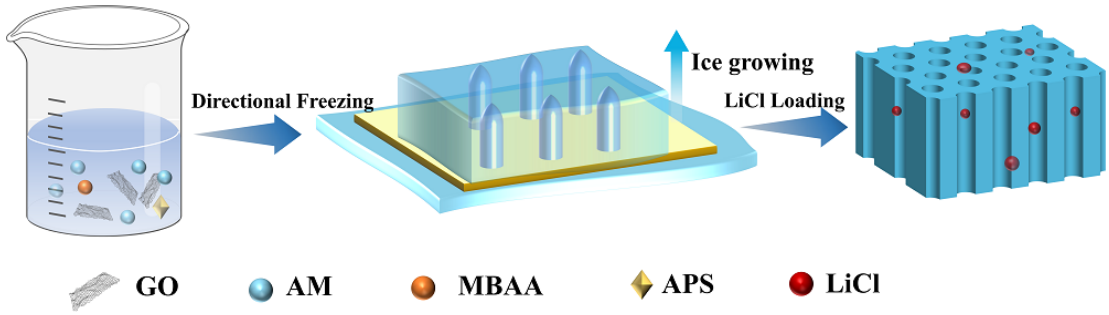


Figure 1. Schematic illustration of the fabrication process of DFHG-Li. GO: graphene oxide; AM: acrylamide; MBAA: N,N'-methylenebisacrylamide; APS: ammonium persulfate; LiCl: lithium chloride.

The SEM images of CHG, DFHG, and DFHG-Li, along with the EDS mapping of DFHG-Li, are presented in Figure 2. The conventional hydrogel CHG exhibits a dense internal structure with irregularly distributed pores of relatively small size (Figure 2a), which is attributed to the non-directional growth of ice crystals during conventional freeze-drying, resulting in disordered and poorly interconnected channels. In contrast, the surface view (Figure 2b) and cross-sectional view (Figure 2c) of DFHG reveal a well-defined directionally aligned channel structure. The channels extend orderly along the freezing direction with uniform pore sizes, and abundant micropores are distributed on the channel walls. Owing to local curvature of ice-crystal-templated pore walls, slight undulation can be observed for individual channel walls, while the overall channels maintain long-range vertical continuity. Additional wide-field side-view SEM micrographs of DFHG (Figure S1 and Figure S2) further verify that the vertically aligned channels penetrate the entire monolith rather than only existing in local regions. The formation mechanism of this oriented structure can be explained as follows: during directional freezing, ice crystals grow preferentially along the temperature gradient direction, leaving behind orderly aligned channels after freeze-drying, while solutes at the ice crystal front are expelled into the interstices between ice crystals, generating micropores on the channel walls. This architecture provides rapid pathways for water transport and gas diffusion, while also increasing the contact area with the atmosphere, which is beneficial for both water vapor adsorption and desorption. These results confirm that the directional freezing strategy can effectively construct ordered porous structures, providing a structural foundation for optimizing adsorption kinetic performance.

The structure and elemental distribution after LiCl loading were characterized by SEM and EDS, with the results presented in Figure 2d,e. The SEM image of DFHG-Li (Figure 2d) shows that the directionally aligned channel structure remained intact without collapse after LiCl loading, and LiCl was uniformly dispersed on the channel walls and within the network without agglomeration. The underlying mechanism can be attributed to the coordination or ion-dipole interactions between the polar groups (e.g., hydroxyl and amide groups) in the hydrogel network and Li^+ and Cl^- ions, which effectively anchor LiCl and suppress its migration and

aggregation during drying. The EDS mapping (Figure 2e) reveals that elements including C, O, N, and Cl are uniformly distributed throughout DFHG-Li, further confirming the successful loading and homogeneous dispersion of LiCl. Collectively, the intermolecular interactions between the hydrogel network and LiCl are key to maintaining structural integrity and achieving uniform dispersion, which provides a structural foundation for the excellent hygroscopic performance of the material.

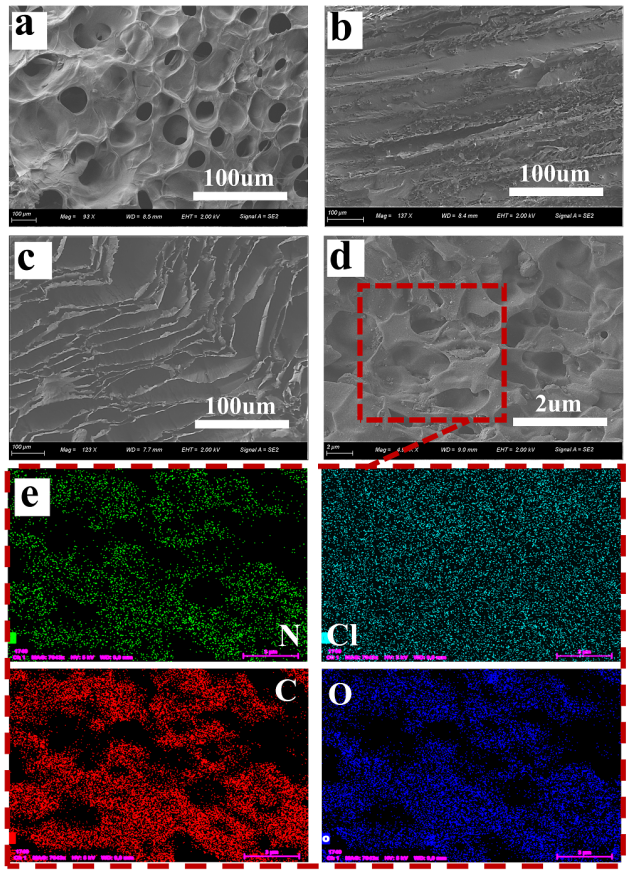


Figure 2. SEM images of CHG (a); DFHG surface (b); DFHG cross-section (c); and DFHG-Li (d); (e) EDS elemental mapping of DFHG-Li. SEM: scanning electron microscopy; CHG: conventional hygroscopic hydrogel.

3.2 Structural characterization and basic properties of freeze-cast hydrogels

The phase structure of the composite materials was characterized by XRD, with the results shown in Figure 3a. DFHG exhibits no distinct diffraction peaks, indicating that the PAM network is amorphous and that directional freezing did not induce polymer crystallization. This is attributed to the fact that during freezing, polymer chains are excluded into the interstices between ice crystals, where chain segment mobility is restricted without ordered arrangement, which is beneficial for maintaining network flexibility and swelling performance. Before water absorption, DFHG-Li displays characteristic diffraction peaks of LiCl at 2θ = 33° and 60°, indicating that LiCl is loaded into the network in a crystalline state. After water absorption, these characteristic peaks disappear, revealing an amorphous structure. The underlying mechanism is that LiCl undergoes deliquescence upon water uptake, dissociating into Li^+ and Cl^- ions and forming an aqueous solution that is uniformly dispersed within the polymer network, thereby disrupting the crystalline structure. This transformation is consistent with the hygroscopic mechanism of LiCl, confirming the water-induced crystalline-to-amorphous transition. The chemical structure and interactions of the composite materials were characterized by FTIR, with the results presented in Figure 3b. DFHG exhibits a broad peak at 3,435 cm^{-1} corresponding to the stretching vibration of $-NH_2$ in AM, a peak at 1,650 cm^{-1} corresponding to C=O stretching vibration, and a peak at 1,452 cm^{-1} corresponding to C-N stretching vibration, confirming the successful polymerization of AM with MBAA to form the PAM network. A weak absorption peak at 1,050 cm^{-1} is attributed to the C-O-C stretching vibration of GO, confirming the successful incorporation of GO. In DFHG-Li, the peak at 3,435 cm^{-1} becomes broader and more intense, which is ascribed to the formation of hydrogen bonds or ion-dipole interactions between Li^+ and the oxygen-containing functional groups (e.g., C=O, C-O-C) in the polymer network, enhancing the O-H/N-H hydrogen bonding network. A characteristic absorption peak of Cl^- appears at 625 cm^{-1}, indicating the successful loading of LiCl and its interaction with the polymer network.

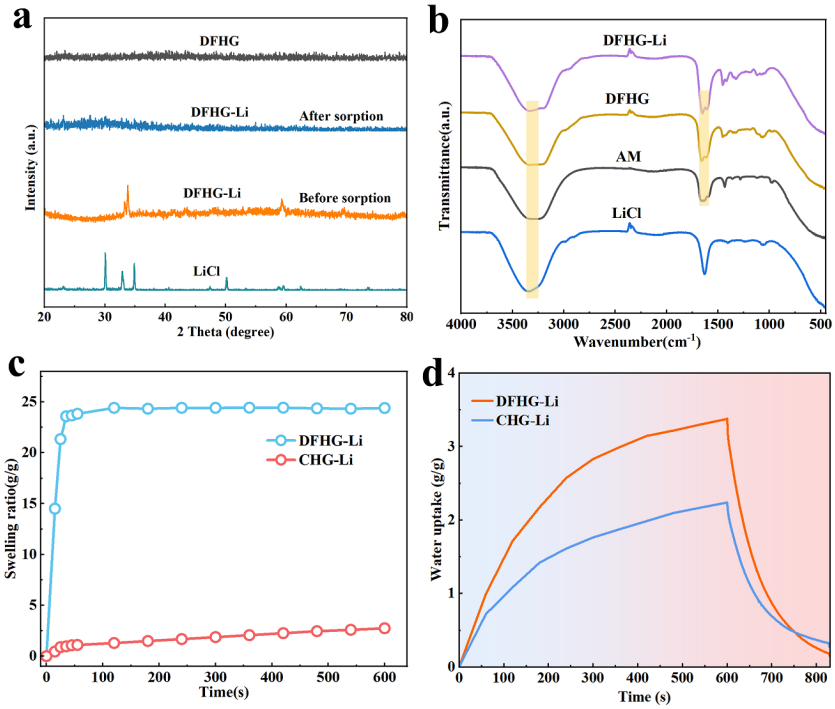


Figure 3. (a) XRD patterns of DFHG and DFHG-Li before and after water absorption; (b) FTIR spectra of DFHG-Li, DFHG, AM, and LiCl; (c) Swelling behaviors of the as-prepared DFHG-Li and CHG-Li in 10 wt% LiCl solution, where DFHG-Li exhibits faster swelling kinetics; (d) Hygroscopic and solar-driven desorption kinetics of DFHG-Li and CHG-Li at 25 °C, showing the moisture uptake at 90% relative humidity and the desorption rate under 1.0 sun illumination. XRD: X-ray diffraction; FTIR: Fourier transform infrared; AM: acrylamide; LiCl: lithium chloride; CHG: conventional hygroscopic hydrogel.

The solution transport performance of the composite materials was evaluated by swelling kinetic curves, with the results shown in Figure 3c. The swelling rate of DFHG-Li in 10 wt% LiCl solution was significantly higher than that of CHG-Li: DFHG-Li reached swelling equilibrium within 3 min, whereas CHG-Li required more than 10 min. The underlying mechanism is that the directionally aligned channel structure in DFHG-Li provides rapid convective and diffusive pathways for the LiCl solution, shortening the time for the solution to reach the interior of the network. In contrast, the irregular and dense pore structure of CHG-Li restricts the solution transport rate. This indicates that the directional channel structure can significantly enhance the mass transfer performance of the material. The adsorption and regeneration performance of the composite materials were evaluated by hygroscopic-desorption kinetic curves, with the results presented in Figure 3d. The moisture adsorption rate, equilibrium adsorption capacity, and desorption rate of DFHG-Li were all significantly superior to those of CHG-Li. The mechanism can be attributed to the fact that during adsorption, the directional channel structure increases the contact area between water vapor and the hygroscopic sites (LiCl), while also providing rapid diffusion pathways for water molecules. During desorption, the ordered channels facilitate the rapid escape of water, preventing water molecules from being trapped within the network. These results confirm that the directional channel structure can synergistically optimize both adsorption and desorption kinetics, endowing DFHG-Li with distinct advantages in terms of high-efficiency adsorption and low-energy regeneration.

Good mechanical properties and thermal stability are two key evaluation criteria for assessing the long-term service reliability of hygroscopic hydrogels and determining their reusability for cyclic atmospheric water harvesting. As shown in Figure 4a, upon removal of the applied compressive load, the DFHG-Li sample rapidly rebounds and recovers its original morphology within a short period, without collapse, cracking, or other undesirable phenomena, demonstrating excellent elastic recovery characteristics. This can be attributed to the synergistic structural effect arising from the vertically aligned directional channels and the chemically crosslinked polymer network within the material: the crosslinked skeleton provides stable mechanical support, while the directional pores can disperse and buffer the applied stress through deformation of the pore walls under external loading, effectively avoiding network fracture and structural damage caused by localized stress concentration, thereby ensuring the integrity of the framework during repeated swelling and dehydration cycles. Supplementary Video S1 further records the compression-rebounding process of DFHG-Li, intuitively demonstrating its excellent elastic resilience under compressive loading. The water droplet wetting test in Figure 4b intuitively reveals the surface wettability of the material. The droplet was completely adsorbed and infiltrated into the matrix within only 0.5 s after contacting the surface, confirming that DFHG-Li possesses excellent superhydrophilicity. Benefiting from the synergistic effect of abundant hydrophilic functional groups in the polymer skeleton and the capillary wicking effect of the pores, the material can rapidly capture gaseous water molecules from the ambient environment, substantially shortening the induction period of water vapor adsorption and enhancing the overall hygroscopic kinetics.

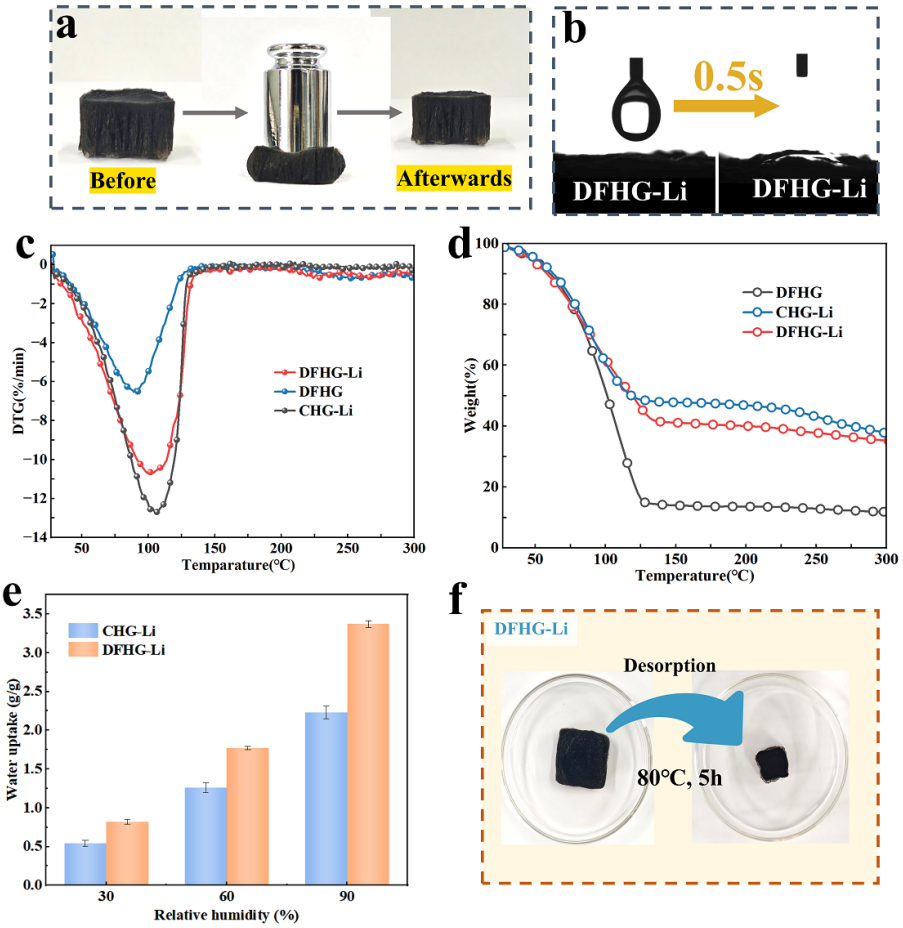


Figure 4. (a) Photographs of DFHG-Li before and after compression; (b) Water adsorption test images of DFHG-Li; (c, d) DTG and TG curves of DFHG, CHG-Li, and DFHG-Li; (e) Water uptake performance of CHG-Li and DFHG-Li at different humidity levels, data are mean ± standard deviation from three independent replicate tests; (f) Macroscopic comparison images of the samples before and after desorption. CHG: conventional hygroscopic hydrogel.

As revealed by the TG and DTG curves in Figure 4c,d, the water evaporation regions of the three samples are distinctly different. Most of the water adsorbed by DFHG-Li exists in the form of free water, with weak interaction forces between the water molecules and the matrix, making them readily desorbed and evaporated upon heating. The DTG results show that the maximum water loss rate of this sample occurs at approximately 100 °C, with a consistently high dehydration rate maintained in the range of 50-130 °C. The total weight loss over the entire temperature range is much higher than that of the DFHG sample without LiCl loading, which is essentially attributed to the strong deliquescent adsorption capacity of LiCl that enables the material to accumulate a large amount of free water. Meanwhile, all tested samples exhibit a slowed weight loss rate at high temperatures above 300 °C, accompanied by a delayed thermal decomposition process of the polymer matrix, demonstrating that the DFHG-series hydrogel matrices possess excellent thermal stability and do not undergo thermal degradation under daily solar-driven photothermal desorption conditions, thus meeting the temperature requirements for practical water harvesting applications. To differentiate various water states inside hydrogels, temperature-segmentation analysis was conducted based on DTG desorption characteristics. Three temperature ranges were defined: free water below 80 °C, weakly bound water from 80 °C to 125 °C, and strongly bound water above 125 °C. Free water weakly interacts with the matrix and desorbs at low temperature. Weakly bound water accounts for the primary weight-loss, whereas strongly bound water demands higher thermal energy for removal. Compared with CHG-Li, DFHG and DFHG-Li show evidently left-shifted desorption peaks and suppressed high-temperature tails. Directional aligned channels provide low-resistance vapor-escape pathways, decrease mass-transfer resistance and modulate water-matrix interfacial interactions. These effects reduce desorption temperature and lower the proportion of strongly bound water, collectively improving photothermal desorption performance.

The water uptake performance curves under different relative humidity conditions (Figure 4e) show that DFHG-Li exhibits significantly higher water uptake than CHG-Li across all humidity environments, and this advantage becomes more pronounced with increasing humidity. Notably, DFHG-Li still delivers considerable moisture harvesting capacity even under dry low-humidity conditions. Specifically, under dry conditions at 30% RH, the water uptake of DFHG-Li reaches 0.89 g/g, which is 1.71 times that of CHG-Li (0.52 g/g); while under high humidity conditions at 90% RH, the water uptake of DFHG-Li reaches as high as 3.37 g/g, far

exceeding that of CHG-Li (2.15 g/g). These results fully demonstrate that DFHG-Li exhibits competitive hygroscopic performance not only under conventional and high humidity conditions but also in arid low humidity environments, significantly broadening its potential application range across different climatic regions. The macroscopic comparison images of the samples before and after adsorption and desorption (Figure 4f) further reveal that the desorbed samples can fully recover to their initial morphology without obvious deformation, damage, or volume shrinkage, once again verifying the favorable structural stability and reusability of DFHG-Li.

3.3 Effect of parameters on hygroscopic performance

Preparation parameters are key factors in regulating the hygroscopic performance of DFHG-Li, among which LiCl concentration, AM content, and the directional channel structure exert the most significant effects. All above-mentioned parameter-dependent hygroscopic measurements in Figure 5 were carried out under 90% RH. The LiCl concentration exhibits a pronounced regulatory effect on the hygroscopic performance of DFHG-Li. As the LiCl concentration increases from low to high, the moisture adsorption rate and equilibrium water uptake first increase significantly, reaching a maximum equilibrium water uptake of 3.37 g/g at 10 wt%. However, upon further increasing the LiCl concentration to 20wt% and 30wt%, the equilibrium water uptake decreases and the adsorption rate slows down considerably. This optimum loading arises from multiple competing factors. An appropriate amount of LiCl supplies abundant hygroscopic sites inside the hydrogel to boost adsorption capacity. FTIR results confirm ion dipole interactions between Li^+ and amide/hydroxyl groups of the PAM network, which act as salt anchoring sites. Once salt content exceeds the anchoring capacity of these polar groups, surplus LiCl tends to crystallize and aggregate. Salt aggregation reduces the effective contact area between water vapor and salt and may partially block internal mass transport pathways. Besides, excessively concentrated immersion solutions can trigger salting-out-induced deswelling of the PAM matrix and even partial collapse of directional pore channels, further impairing hygroscopic performance. Taking these competing effects into consideration, 10 wt% was therefore determined as the optimal LiCl loading concentration, which balances sufficient hygroscopic sites, unobstructed mass transport pathways, and intact hydrogel architecture.

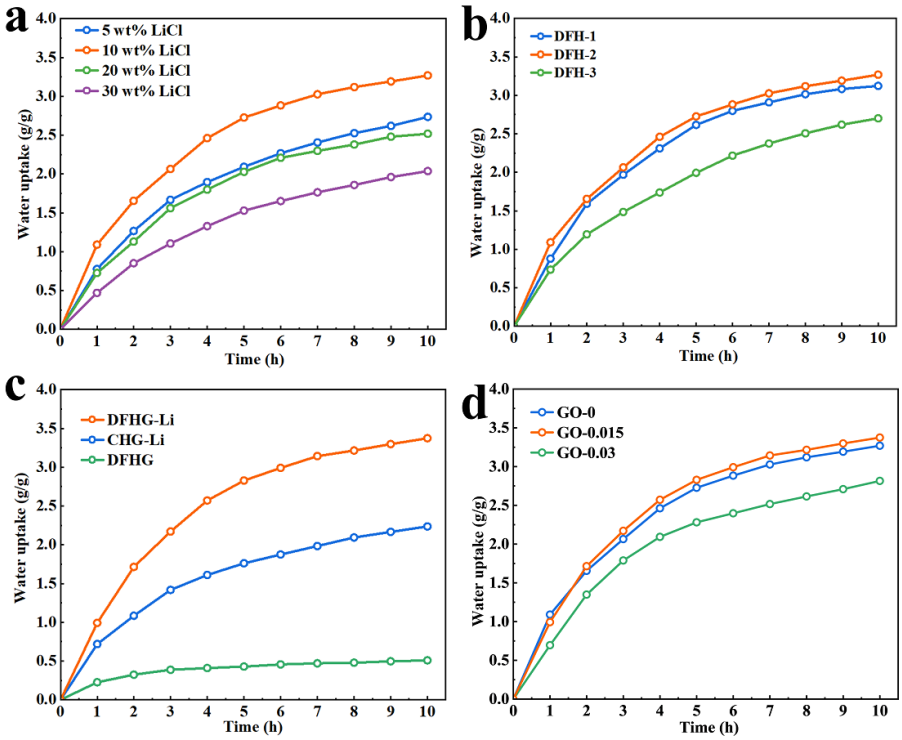


Figure 5. (a) Water uptake performance of DFHG-Li with different salt contents at 25 °C and 90% RH; (b) Water uptake performance of DFHG-Li with different AM contents at 25 °C and 90% RH; (c) Water uptake performance of DFH-Li, CH-Li, and DFH at 25 °C and 90% RH; (d) Water uptake performance of DFHG-Li with different GO contents at 25 °C and 90% RH. AM: acrylamide; GO: graphene oxide.

The AM content also exerts a significant regulatory effect on the hygroscopic performance of DFHG-Li. When the AM mass fraction increases from 6 wt% to 9 wt%, both the moisture adsorption rate and equilibrium water uptake of DFHG-Li show an upward trend. However, upon further increasing the AM content to 12 wt%, the equilibrium water uptake decreases markedly and the time required to reach adsorption equilibrium is prolonged. This variation can be attributed to the evolution of the polymer network structure: a moderate AM content (9 wt%) enables the formation of an intact and stable three-dimensional network, providing sufficient loading sites for LiCl and ensuring rapid diffusion channels for water molecules. When the AM content is excessively high, the crosslinking density of the polymer increases, leading to reduced network porosity and increased resistance to water diffusion, thereby

suppressing the adsorption kinetics. Conversely, when the AM content is too low, the polymer network becomes incomplete and defective, making it difficult to effectively confine LiCl, which results in salt leakage and a decline in adsorption capacity. Accordingly, the optimal AM content was determined to be 9 wt%.

The synergistic effect of the directional channel structure and LiCl loading is central to the excellent hygroscopic performance of DFHG-Li. By comparing hydrogel samples with different structures and compositions, it is evident that the hygroscopic performance of DFHG-Li is significantly superior to that of conventional hydrogels without directional structure and directionally frozen hydrogels without LiCl loading. This result indicates that both the directional channel structure and LiCl loading play critical roles in enhancing the hygroscopic performance: the directional channel structure provides rapid pathways for water transport and accelerates the mass transfer process, while LiCl supplies abundant hygroscopic sites. Their synergistic interaction substantially enhances the overall hygroscopic performance. In contrast, hydrogels without directional structure suffer from poor mass transfer efficiency and consequently inferior hygroscopic performance, while directionally frozen hydrogels without LiCl loading rely solely on the physical adsorption of the polymer network, resulting in extremely limited adsorption capacity.

3.4 Photothermal performance and cyclic stability

The schematic diagram of the adsorption-desorption process of DFHG-Li is illustrated in Figure 6. During the adsorption stage, water vapor from the atmosphere first undergoes physical adsorption on the hydrophilic groups (e.g., -NH_2, -COOH, etc.) and LiCl on the hydrogel surface, forming an adsorbed film. Subsequently, LiCl chemically reacts with the adsorbed water vapor to form LiCl·nH_2O hydrates, which gradually deliquesce into an aqueous LiCl solution. Driven by the concentration gradient, this deliquesced solution rapidly diffuses through the directional channels into the interior of the hydrogel, where it is encapsulated and stored within the polymer network[25]. Meanwhile, the surface adsorption sites are continuously regenerated, enabling sustained capture of water vapor from the atmosphere. During the desorption stage, GO converts solar energy into thermal energy under sunlight irradiation, elevating the surface temperature of the hydrogel and thereby reducing the adsorption affinity of the material toward water molecules. Concurrently, the directionally aligned channel structure accelerates both the transfer of heat to the interior and the diffusion of water vapor to the surface, facilitating rapid water evaporation. The evaporated water vapor then condenses on the inner walls of the water collection device to form fresh water, thereby completing the water harvesting process.

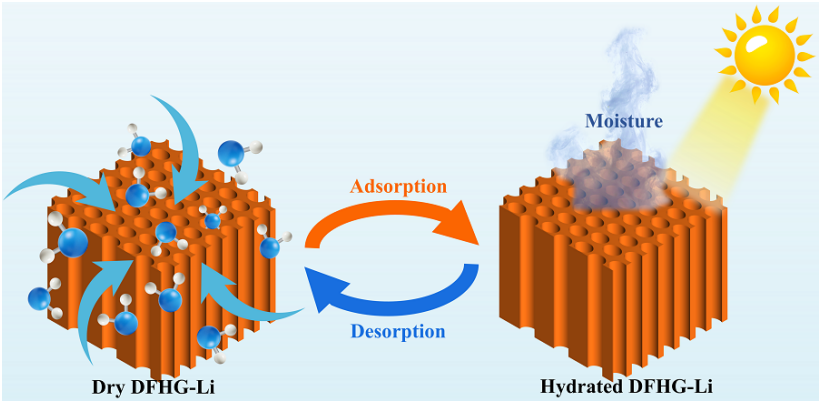


Figure 6. Schematic illustration of the water adsorption/desorption process.

Photothermal conversion efficiency and cyclic stability are core indicators for evaluating the practicality of adsorbents. Figure 7 presents the comprehensive performance of DFHG-Li in these two aspects. The schematic diagram of the water desorption setup (Figure 7a) illustrates the device configuration for outdoor water harvesting experiments, with its operational principle based on the "adsorption-photothermal desorption-condensation" cyclic process of the directionally frozen hydrogel, thereby achieving atmospheric water harvesting.

Excellent photothermal conversion capability is crucial for solar driven desorption systems. As shown in Figure 7b, benefiting from the outstanding light absorbing properties of GO, DFHG-Li exhibits significantly superior light absorption performance in the UV-Vis-NIR absorption spectra compared with GO-free DFH-Li. The supplemented temperature-time curves in Figure 7c further verify the critical photothermal role of GO under 1.0 sun illumination. DFHG-Li shows rapid surface temperature increase and reaches 51.2 °C within 15 min, while GO-free DFH-Li achieves a much lower surface temperature under the same irradiation condition. In addition, the temperature gap between DFHG-Li and CHG-Li indicates that vertically aligned channels facilitate inward heat transport inside the hydrogel matrix, which is favorable for subsequent water desorption. The infrared thermal images in the inset further demonstrate that after hydration at 90% RH for 8 h, DFHG-Li exhibits a significant surface temperature increase and substantial water evaporation upon 1.0 sun irradiation for 70 min, evidencing the excellent photothermal conversion performance of the material and its capability to drive desorption. The temperature variation curves under different light intensities are presented in Figure 7d. With

increasing light intensity, both the heating rate and equilibrium temperature of DFHG-Li are significantly enhanced, reaching 57.2 °C under 1.5 sun illumination. The underlying mechanism is that higher light intensity provides greater energy input, accelerating the photothermal conversion process of GO, thereby enabling desorption under various environmental conditions and demonstrating the favorable adaptability of the material to different light conditions.

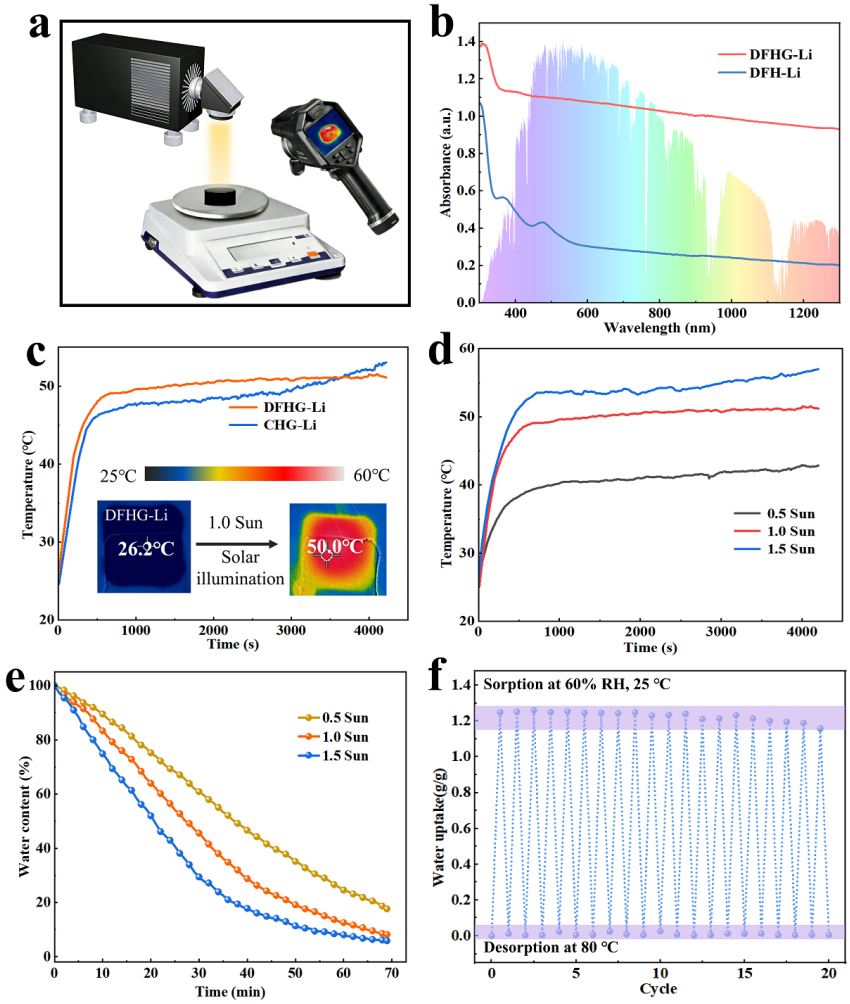


Figure 7. (a) Schematic diagram of the water desorption setup; (b) UV-Vis-NIR absorption spectra of DFHG-Li and DFH-Li; (c) Temperature evolution of DFH-Li, CHG-Li and DFHG-Li as a function of time under 1.0 sun illumination, with the inset showing infrared thermal images of DFHG-Li hydrated at 90% RH for 8 h before and after 70 min of 1.0 sun irradiation; (d) Temperature variation of DFHG-Li under different solar light intensities; (e) Water release amount of DFHG-Li under different irradiation intensities; (f) Moisture uptake retention after 20 cycles. CHG: conventional hygroscopic hydrogel.

The water release curves under different light intensities are shown in Figure 7e. Higher light intensity leads to greater desorption rates and total water release amounts from DFHG-Li: the desorption rate reaches 91.5% within 70 min under 1.0 sun illumination and 93.7% under 1.5 sun, while it still attains 81.3% even under weak light conditions of 0.5 sun. This trend originates from the faster photothermal heating and stronger driving force for water evaporation under higher light intensities, indicating that the desorption performance of DFHG-Li is highly responsive to light intensity, allowing flexible adjustment of water harvesting strategies according to actual light conditions. The cyclic stability test is shown in Figure 7f. After 20 adsorption-desorption cycles, the moisture uptake retention rate of DFHG-Li remains above 89%. The underlying mechanism is that the spatial confinement effect of the polymer network on LiCl effectively suppresses salt leakage and agglomeration, demonstrating that the material possesses excellent cyclic stability and can meet the requirements for long-term practical applications.

4. Conclusion

This study addresses the low mass transfer efficiency and high desorption energy consumption of conventional hygroscopic hydrogels by fabricating a DFHG-Li via directional freezing-assisted polymerization, leveraging a dual-network structure synergistically reinforced by hydrogen bonding. The vertically interconnected channels significantly optimize internal mass transfer, enabling DFHG-Li to reach swelling equilibrium within 3 min, far outperforming disordered systems. At 90% RH, the equilibrium

uptake reaches 3.37 g/g, 1.57 times that of the control. The incorporation of GO provides excellent photothermal conversion, raising the surface temperature to 51.2 °C within 15 min under 1.0 sun illumination and achieving a desorption rate of 91.5% within 70 min. Benefiting from the dual-network and hydrogen bonding synergy, DFHG-Li retains over 89% of its water harvesting capacity after 20 cycles. While the ordered channels effectively mitigate mass transfer barriers for water harvesting, this system has inherent practical limitations in terms of real-world water yield and large-scale manufacturing. Further efforts should be devoted to optimizing heat mass transfer synergy to promote its practical deployment for atmospheric water harvesting.

Supplementary materials

The supplementary material for this article is available at: Supplementary materials.

Declarations

Acknowledgements

The authors acknowledge the support from the Discipline of Shanghai—Materials Science and Engineering, and Shanghai Engineering Research Center of Advanced Thermal Functional Materials.

Authors contribution

Yu J: Writing-original draft, data curation.
Wang D: Investigation, formal analysis.
Li Y: Writing-review & editing, supervision, conceptualization.
Xie H: Resources, project administration.
Yu W: Funding acquisition, writing-review & editing.
Wang L: Writing-review & editing, funding acquisition, conceptualization.

Conflicts of interest

The authors declare no conflicts of interest.

Ethical approval

Not applicable.

Consent to participate

Not applicable.

Consent for publication

Not applicable.

Availability of data and materials

Data will be made available on request.

Funding

The authors acknowledge funding from Shanghai Science and Technology Commission Capacity Building Program for Local Institutions (Grant No. 21010500600), National Natural Science Foundation of China (Grant No. 52276074) and Shanghai Sailing Program (Grant No. 21YF1414200).

Copyright

© The Author(s) 2026.

References

1. Musie W, Gonfa G. Fresh water resource, scarcity, water salinity challenges and possible remedies: A review. Heliyon. 2023;9(8):e18685. [DOI][PubMed][PMC]
2. Onyena AP, Sam K. The blue revolution: Sustainable water management for a thirsty world. Discov Sustain. 2025;6(1):63. [DOI]
3. Boretti A. Global water insecurity accelerating: A multidimensional reassessment integrating scarcity, pollution, geopolitics, and equity towards 2050. World Water Policy. 2026;12(1):e70062. [DOI]

4. Lee Y, Fan S, Yang S. Nature-inspired design strategies for efficient atmospheric water harvesting. Adv Mater. 2025;37(51):e19362. [DOI][PubMed][PMC]
5. Wang P, Xu J, Bai Z, Wang R, Li T. Designing next-generation all-weather and efficient atmospheric water harvesting powered by solar energy. Energy Environ Sci. 2025;18(14):7005-7022. [DOI]
6. Guan W, Deng F, Lei C, Chen Z, Wang R, Yu G. Toward practical atmospheric water harvesting technologies. Sci Adv. 2026;12(23):eaef4164. [DOI][PubMed][PMC]
7. Sadek S, Zayed ME, Li C, Rehman S, Deng S. Sustainable freshwater production using sorption-based atmospheric water harvesting: Sorbent materials, system design configurations, thermodynamic models, and future perspectives. Int Commun Heat Mass Transf. 2026;170:110049. [DOI]
8. Ehtisham M, Saeed-Ul-Hassan M, Poater A. A comprehensive review of approaches, systems, and materials used in adsorption-based atmospheric water harvesting. Sci Total Environ. 2025;958:177885. [DOI][PubMed]
9. Wu X, He J, Lao Z, Ning X, Zhu J, Zhang L. Recent progress on composite hydrogels and their integrated devices for atmospheric water harvesting. Compos Commun. 2025;59:102601. [DOI]
10. Liu X, Li J, Zhang Z, Peng H, Liu J, Song N, et al. Molecular engineering-enabled design of POMs-based thermosensitive hygroscopic hydrogels for high-efficiency atmospheric water harvesting. Chem Eng J. 2026;531:174006. [DOI]
11. Graeber G, Díaz-Marín CD, Gaugler LC, El Fil B. Intrinsic water transport in moisture-capturing hydrogels. Nano Lett. 2024;24(13):3858-3865. [DOI][PubMed][PMC]
12. Lu R, Tang H, Wu X, Guo C, Feng S, Zhao D. Sorption kinetics of salt-embedded bulk and porous hydrogels: A mass transfer analysis. Int J Heat Mass Transf. 2026;256:128113. [DOI]
13. Song M, Cheng T, Li Y, Huang D, Huang X, Xie H, et al. Spongy hygroscopic hydrogels for efficient atmospheric water harvesting over a wide humidity range. J Clean Prod. 2024;461:142661. [DOI]
14. Zhao Y, Guan W, Yu G. Challenges and strategies toward sustainable atmospheric water harvesting. Acc Mater Res. 2025;6(11):1332-1343. [DOI]
15. Bhutra K, Avhad M, Bhilpawar O, Awchare P, Deore M, More A. Natural polymer-based cryogels: Synthesis, properties, and applications: A review. Starch Stärke. 2026;78(6):e70233. [DOI]
16. Jain E, Zhang K, Mishra Tiwari R. Properties and characterization of cryogels: Structural, mechanical, and functional insights. ACS Omega. 2025;10(33):36771-36787. [DOI][PubMed][PMC]
17. Charlie R, Loïc F, Laurent C, Jean-Eudes M, Sana EM, Benoit D, et al. From water molecule mobility to water-resistance of swollen oriented and non-oriented cellulose nanofibril cryogels. Cellulose. 2024;31(17):10191-10207. [DOI]
18. Luo M, Liu J, Yao J, Zhao P, Liu S, Liao S, et al. From aligned structures to enhanced performance: A review on freeze-cast hydrogels and functional applications. Chem Commun. 2026;62(25):6677-6695. [DOI][PubMed]
19. Hu S, Qin W, Chen M, Zhai H, Bi Y, Wang Y, et al. Hygroscopic gels with Li+ leak-resistance and fast-cycling performance via multidentate ion locking and hierarchical pore design. Chem Eng J. 2026;543:178566. [DOI]
20. Yang X, Shan H, Chen Z, Wang R. Macroporous zwitterionic hydrogel sponge with enhanced kinetics by in-situ UV cryogelation for efficient water production. Adv Funct Mater. 2026;36(45):e20072. [DOI]
21. Fang Z, Xu H, Xu Q, Meng L, Lu N, Li R, et al. High efficiency of formaldehyde removal and anti-bacterial capability realized by a multi-scale micro-nano channel structure in hybrid hydrogel coating cross-linked on microfiber-based polyurethane. ACS Appl Mater Interfaces. 2023;15(28):34108-34119. [DOI][PubMed]
22. Entezari A, Ejeian M, Wang R. Super atmospheric water harvesting hydrogel with alginate chains modified with binary salts. ACS Mater Lett. 2020;2(5):471-477. [DOI]
23. Li M, Wang T, Hou XG, Zhang XS. Preparation of polyvinyl alcohol/sodium alginate composite aerogel and its application in efficient seawater desalination. Acta Mater Compos Sin. 2023;40(10):5726-5735. Chinese. [DOI]
24. An N, Zhang W, Wang P, Li Q, Qiu J. Hydrogels with engineered functions for solar-driven technologies in water-energy-environment. Nano Energy. 2026;151:111798. [DOI]
25. Zhu Z, Yu H, Wang L, He J, Zhang Y, Wang Y, et al. Advances in hygroscopic hydrogels for atmospheric water harvesting applications. J Environ Chem Eng. 2025;13(5):119047. [DOI]
26. Liu Q, Qin C, Solomin E, Chen Q, Wu W, Zhu Q, et al. Research progress on the development of new nano materials for solar-driven sorption-based atmospheric water harvesting and corresponding system applications. Nano Energy. 2023;115:108660. [DOI]
27. Zhu P, Yu Z, Sun H, Zheng D, Zheng Y, Qian Y, et al. 3D printed cellulose nanofiber aerogel scaffold with hierarchical porous structures for fast solar-driven atmospheric water harvesting. Adv Mater. 2024;36(1):e2306653. [DOI][PubMed]
28. Li J, Xu C, Chen L, Zhang X, Zhu M, Cheng Y. Tandem atmospheric water harvesting and passive cooling enabled by hygroscopic biopolymer-based aerogels. Adv Funct Mater. 2025;35(31):2423063. [DOI]
29. Lu J, Yan J, Pei F, Niu Z, Li J, Han G, et al. Shrinkage-resistant thermo-responsive hygroscopic hydrogel toward ultra-rapid cycling atmospheric water harvesting. Adv Funct Mater. 2025;35(42):2505359. [DOI]
30. Zhu M, He G, Wang Z, Chen J, Fu X, Yang H, et al. MOF-801 enabled rapid-cycling atmospheric water harvester with vertically aligned photothermal channel. J Environ Chem Eng. 2024;12(5):113815. [DOI]
31. Gao C, Yu D, Zhu L, Wei H, Zhang L, Zhou M, et al. Robust bioinspired microcellular and micro-nanochannel photothermal aerogels for high-efficiency atmospheric water harvesting. ACS Nano. 2025;19(45):39292-39302. [DOI][PubMed]

32. Katulkar A, Kosta DK, Tiwari S, Bajpai M, Bajpai SK. Performance analysis of efficient and cost effective hydrogels for thermal regulation strategy. Discov Polym. 2026;3(1):4. [DOI]
33. Yan J, Li W, Yu Y, Huang G, Peng J, Lv D, et al. A Polyzwitterionic@MOF hydrogel with exceptionally high water vapor uptake for efficient atmospheric water harvesting. Molecules. 2024;29(8):1851. [DOI][PubMed][PMC]
34. Ma LF, Chen DM, Xu Y, Tao CJ, Fan YB. Effect of molecular weight selection and relative humidity on the moisture absorption and desorption behavior of poly(N-isopropylacrylamide)-based hydrogels. Chin J Polym Sci. 2025;43(11):2061-2072. [DOI]

Publisher's Note

Science Exploration remains a neutral stance on jurisdictional claims in published maps and institutional affiliations. The views expressed in this article are solely those of the author(s) and do not reflect the opinions of the Editors or the publisher.